JGR Space Physics

RESEARCH ARTICLE
10.1029/2020JA028619

Key Points:

- MMS current density via particles at the electron DES time resolution is NOT model independent
- Four theorems are presented to justify point 1, including demonstrating that Nyquist's condition has been violated at present in this MMS data product
- Those desiring current measurements from MMS should recompute them properly respecting the DIS ion subsystem's Nyquist limit on its frequency content. It is 5 times slower than the Nyquist condition for DES samples of moments

Correspondence to:
J. D. Scudder,
Jack-scudder@uiowa.edu

Citation:
Scudder, J. D. (2021). Measuring particle current density J on NASA's magnetospheric multiscale mission (MMS). *Journal of Geophysical Research: Space Physics*, *126*, e2020JA028619. https://doi.org/10.1029/2020JA028619

Received 25 AUG 2020
Accepted 11 NOV 2020

© 2020. American Geophysical Union. All Rights Reserved.

Measuring Particle Current Density J on NASA's Magnetospheric Multiscale Mission (MMS)

J. D. Scudder[1]

[1]Department of Physics and Astronomy, University of Iowa, Iowa City, IA, USA

Abstract A theorem is proved that the minimum Nyquist compatible cadence $\Delta\tau$ for subsequent model free determinations of current density **J** by magnetospheric multiscale (MMS) instrumentation is the cadence of the *ion* plasma subsystem DIS of the fast plasma investigation (FPI). A sample of published discoveries and signatures of magnetic dissipation associated with collisionless magnetic reconnection at the noon magnetopause are reviewed that utilize observations of the variable $\mathbf{J}_{\text{plasma}}(t)$ reported at the electron DES subsystem cadence which is always $\Delta\tau/5$. Nyquist's theorem precludes a unique interpolation of DIS observations to the DES cadence, casting a serious shadow on rumored interpolation strategies said to allow measurement of $\mathbf{J}_{\text{plasma}}$ at the DES cadence. The theorems and corollary are properties only of the FPI flight hardware and do not depend on peculiar plasma conditions for their conclusions. Determinations of **J** with measured scale lengths require a still slower cadence, twice that of the DIS subsystem. A rationale is still missing for the present MMS approach for determining $\mathbf{J}_{\text{plasma}}$ at the DES cadence.

1. Introduction

Since the influential review by Vasyliunas (1975), the physics of the electron diffusion region (EDR) of collisionless magnetic reconnection (CMR) has been modeled as dominated by electron inertial scale physics; depending on the size of β_e, current density channels with e-folding widths either the thermal electron gyroradius or skin depth scale were suggested as indicative of penetrating the largely unknown region of the EDR.

An appreciation of the challenges for identifying such layers and finding the EDR penetration is shown in Figure 1 that indicates in panel (a) the empirically determined probability distributions, $\mathbb{P}(\mathbb{L})$, in the noon magnetopause regime for different sized electron inertial scales $\mathbb{L}$: the electron gyroradius, ρ_e, and its skin depth, d_e, based on the data studies of Wang et al. (2012) and Haaland et al. (2020) and (b) the probability distribution for the transit time $\mathbb{TT}$ of these scales using an MMS data-based empirical probability distribution of measured magnetopause speeds, V_{MP}, in this regime (Haaland et al., 2020).

Mean values and errors of observables used in these curves are $n_e = 15 \pm 3$/cc, $T_e = 70 \pm 15$ eV (Wang et al., 2012) and $|B| = 40 \pm 12$ nT, $V_{MP} = 35 \pm 5$ (Haaland et al., 2020). Since $\mathbb{L}$ and $\mathbb{T}$ can involve multiple variables, sampled $\pm 3\sigma$, non-Gaussian behavior is anticipated, especially in inset (a) when considering the possibility of the weakest magnetic fields. These probabilities, based on measurements typical for the noon magnetopause, are representative of the near noon sector of the initial reconnection surveys performed NASA's magnetospheric multiscale (MMS) mission launched in 2015. The electron skin depth, d_e is generally marginally larger than the expected electron gyroradius, ρ_e. However, d_e is small with most probable values in this region of $\overline{d}_e \simeq 1 - 3$km, similar to skin depths of initial science results layers discussed (Burch et al., 2016). These scales are approximately 100 times smaller than the commonly encountered ion gyroradius scale of the typical magnetopause current layer.

The probabilities of transit times $\mathbb{TT}$ of the inertial lengths $\mathbb{L}$ compiled in Figure 1b are determined as

$$\mathbb{TT}(\mathbb{L}) \equiv \frac{\mathbb{L}}{V_{MP}}. \tag{1}$$

Having values of several tens of milliseconds, the expected transit times $\mathbb{TT}$ in inset (b) testify to the very high time resolution required for identifying structures with inertial length scales.

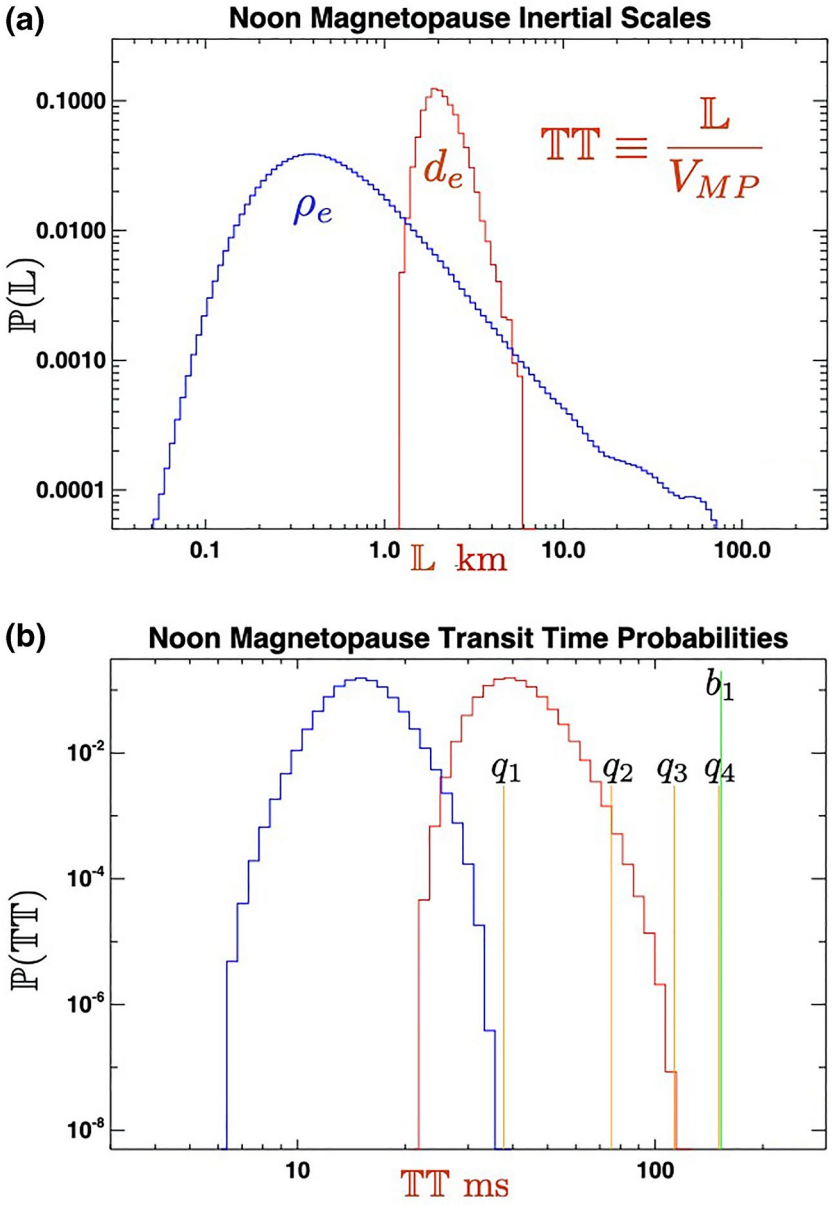

Figure 1. (a) Probability distribution of electron inertial scales, $\mathbb{L}$, at noon magnetopause. (b) Probability distribution of transit times, $\mathbb{TT}$, of inertial layers over the spacecraft (same color coding). In inset (b), the time labeled $b_1 = 150$ ms is the data collection interval needed to produce *one* 3-D ion characterization in *burst mode*. The times labeled q_j correspond to the cumulative duration $j \times 37.5$ ms for j successive 3-D ion characterizations in the rarely available *qburst mode* data format.

Given that the electron gyroradius and skin depths are comparable, EDR detection strategies prior to MMS launch were tested analyzing particle in cell (PIC) simulations for signatures of electron demagnetization reflected in signatures of agyrotropy of the electron pressure tensor (Scudder & Daughton, 2008) and electron thermal speed Mach numbers of $\mathcal{O}(1)$. The spatial occurrence of these signatures was contrasted with the unequivocal EDR locales defined mathematically from the PIC code's vector potential. Prior to MMS launch, both signatures were used in 2012 with Polar data for the first time in space to identify the EDR using its expected properties illustrated in a relevant PIC simulation (Scudder et al., 2012).

A survey of EDR detection strategies and their possible nonunique signatures was reviewed in 2014, probing PIC simulations with known magnetic topologies to ascertain spacecraft observable signatures

(Scudder, 2016); electron demagnetization effects were also shown to occur along the separatrices, well removed from the mathematically defined separator, illustrating in a controlled way the complexity of spacecraft identification of the EDR.

As planned in 2005, NASA's MMS four spacecraft mission was focused on a number of kinetic scale phenomena embedded in large-scale geophysical hydromagnetic flows found in earth orbit. Elucidating the physics of the EDR about the separator including the EDR was a central MMS objective in its CMR effort that required markedly enhanced time resolution to (i) find, (ii) resolve, and (iii) characterize electron inertial scale layers at the magnetopause. With unknown properties, even the finding of the EDR was a nontrivial objective. For this purpose, using model-independent determinations of electrical current density **J** with inertial scale lengths was thought to be highly desirable for identifying the EDR. In this way, the MMS CMR focus sought to experimentally determine the properties of empirically located EDRs, hoping to contrast them with, and thus test, theoretically suggested expectations of their role in collisionless reconnection.

To experimentally evaluate Vasyliunas's theoretical insight required (i) the ability to measure the quasi-static current density $\mathbf{J}(t)$ rapidly on the spacecraft in a model-independent way with sufficient temporal spacing, $\Delta\tau$ and (ii) to be able to *measure the spatial scale* of the skin current layer formed by **J**.

This paper looks at these objectives and how they have been addressed with MMS data products and publications since launch. Several serious impediments to carrying out this program of model-independent measurements are identified. A number of first principles theorems are proven, some based on Nyquist's theorem from information theory, demonstrating that the fastest (burst mode) cadence for model-independent **J** determinations is $\Delta\tau = 150$ ms, 5 times slower than the MMS data product $\mathbf{J}_{\text{particle}}$ plotted and geophysically interpreted with 30 ms time resolution by Burch et al. (2016). Specializing the theorem to the much rarer *qburst mode* data products demonstrates that the fastest model-independent current density measurement possible is at $\Delta\tau = 37.5$ ms, rather than the 7.5 ms cadence reflected in publications using qburst data (e.g., Webster et al., 2018).

The minimum spacecraft elapsed time for measuring the scale of the resolved current density is shown to be $2\Delta\tau$, using the given data mode dependent values of $\Delta\tau$ for the current density. The probability of the electron skin depth transit durations at the noon magnetopause has been used to demonstrate the negligible probability to date that skin depth scale current densities have been measured in a model-independent way. Because of the Nyquist theorem violations implicit in the MMS data product $\mathbf{J}_{\text{plasma}}$, neither it nonzero size nor its computed orientation is suitable for scientific discovery.

2. Inertial Scale Length for J = |J|

Skin surface currents are frequently modeled (Jackson, 1975) with a 1-D spatial form

$$\mathbf{J}_{skin} \simeq \frac{\mathbf{A}_o \Theta(x)}{d_e} \exp\left(-\frac{x}{d_e}\right), \tag{2}$$

where the e-folding length d_e is the skin depth, $\Theta(x)$ is the Heaviside step function, and $\mathbf{A}_o$ is a constant vector related to the size of the tangential size of the magnetic field, **H**, at $x = 0^-$.

The spatial profile of Equation 2 is shown in Figure 2a in the elapsed time format, where uniform relative motion with speed V_{MP} has been assumed to replace the skin depth with the transit time of the skin depth, $\mathbb{TT}$, and the distance x from the origin is replaced by the corresponding time since crossing the peak skin current:

$$|\,\mathbf{J}\,|_{skin}\,(t) \simeq J_o \Theta(t) \exp\left(-\frac{t}{\mathbb{TT}}\right) \tag{3}$$

In this usual model, the skin current rises as a step function at $t = 0$ to a peak value from which it exponentially decays with elapsed time from the peak.

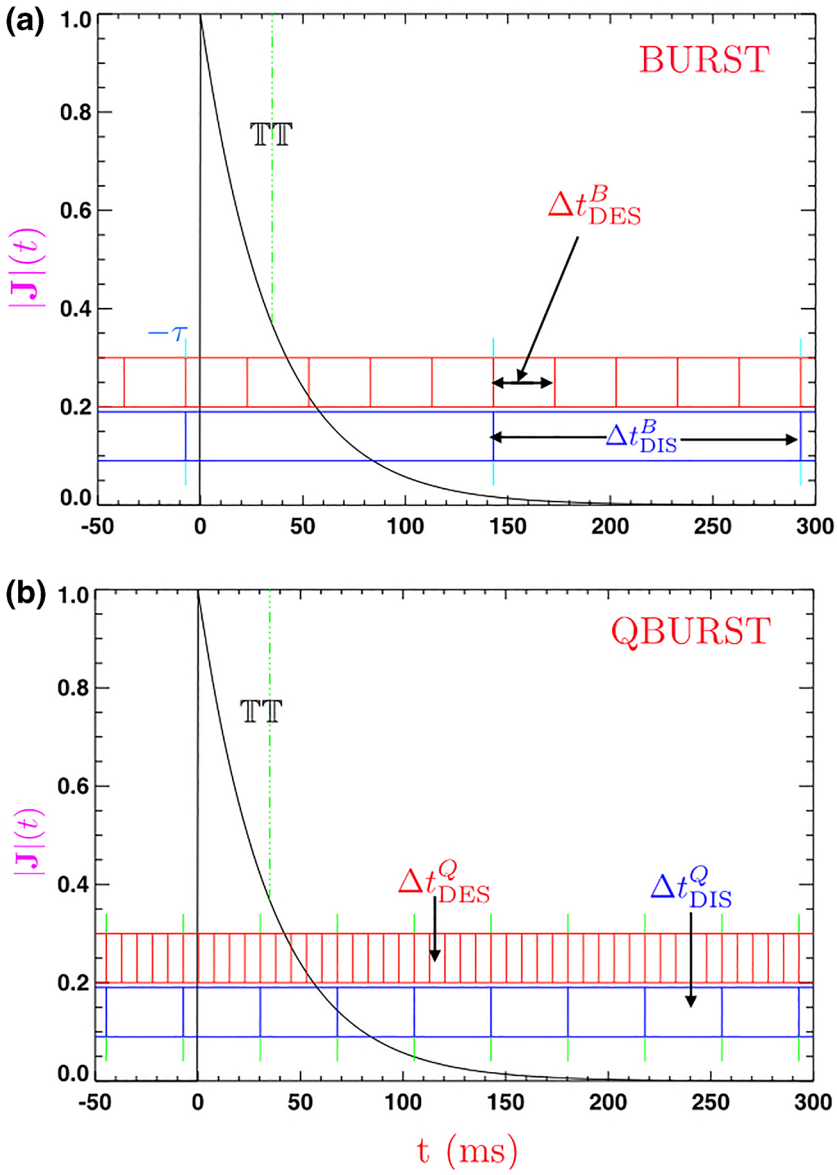

Figure 2. Time profile for transiting a skin current profile (arbitrary units) is the same for both panels. Depicted e-folding *time* is the spacecraft transit time $\mathbb{TT}$, using the modal value for it in Figure 1b. Panel (a) pertains to the default *burst* format data products planned at launch (Pollock et al., 2016). Panel (b) pertains to *qburst* format data products (Rager et al., 2018). Blue (red) rectangles indicate by their width the velocity space acquisition time required to produce *one* replication of 3-D moments for the DIS (DES) plasma subsystems of fast plasma investigation (FPI) (Pollock et al., 2016) for the panel's format.

Because it takes a time $\Delta\tau$ for a plasma instrument to gather adequate information to perform a 3-D moment over velocity space, the observables are essentially time averages of the witnessed variations of $\mathbf{J}(t)$ over $t \pm \Delta\tau/2$. Such average vectors are then available with a time spacing, or duty cycle, $\Delta\tau$ between subsequently tagged readings from the plasma instrument. Thus

$$\mathbb{J}_k \equiv \frac{1}{J_o \Delta\tau}\left|\int_{t_k-\Delta\tau/2}^{t_k+\Delta\tau/2}\mathbf{J}(t')dt'\right|, \tag{4}$$

where the subscript k on the scaled current density modulus $\mathbb{J}_k$ identifies the center time t_k of the data collection interval indicated.

To measure the spatial scale L of the current density $\mathbb{J}$ requires estimating

$$L_x^{-1} \equiv \mid \nabla \ln \mathbb{J} \mid . \tag{5}$$

In the first finite difference approximation for L, two independent adjacent average readings of $\mathbb{J}$ are required:

$$\begin{aligned} L &\simeq \frac{\mid \Delta \mathbf{x} \mid}{\ln \mathbb{J}_2 - \ln \mathbb{J}_1} \\ &= \left| \frac{V_{MP} \Delta \tau}{\ln(\mathbb{J}_2 \,/\, \mathbb{J}_1)} \right|. \end{aligned} \tag{6}$$

The numerator of the finite difference in Equation 6 is the spatial separation between the time *labels* for the *successive, monotonic* determinations of $\mathbb{J}_k$.

The minimum total measurement time interval for measuring the current density's scale (by first finite difference) is thus $2\Delta\tau$, twice the basic aliasing time for the fast plasma investigation (FPI) instruments to determine *one model-independent estimate* of **J**. The data acquisition interval for both estimates $\mathbb{J}_k$ must be entirely on the same side of the decaying current profile (cf. Figure 2). This construction proves:

Theorem I. "If $\Delta\tau$ is the minimum spacecraft elapsed time to determine one estimate of **J** in a model-independent way, then the minimum time to determine the *scale* of **J** is $2\Delta\tau$."

3. $\Delta\tau$ for Model-Independent J

This next section proves a theorem that relates the *lower limit size* of $\Delta\tau$ for **J** in Theorem I to the hardware characteristics of the FPI subsystems (Pollock et al., 2016).

The driving factor for the design of the MMS fast plasma instrument (FPI) (Pollock et al., 2016) was the requirement to measure quasi-stationary current density **J**, as defined by Maxwell (cf. Equation 7), as the difference between ion and electron charged number fluxes. This approach was taken after considering (i) that the expected narrow ≃1–3 km skin depth scales (recovered in Figure 1a) of the expected EDR current channels at the noon magnetopause would render the curlometer approach (Dunlop et al., 2002) ineffective given the planned 4-spacecraft minimum spacing of 10 km (Burch et al., 2016); (ii) that variations in the magnetic field alone placed limits only on the change of integrated current ΔI, rather than on the desired current *density*, **J**; and (iii) that other approaches such as Minimum Faraday Residue (Khrabrov & Sonnerup, 1998) might misleadingly involve incorrect geometrical assumptions for exploratory EDR measurements.

The plasma fluxes for the **J** determination were to be obtained from two specialized plasma subsystems, the DES and DIS, where the subsystem acronyms stand for Dual X Spectrometers, where X is either E or I for the electron and ion subsystem, respectively. Composition is measured on MMS, but at a much slower cadence than the DIS. The routine $\mathbf{J}_{\text{plasma}}$ determinations reported in the literature do not account for ion composition or of electron charge fluxes implied by solid-state electron energy observations that have their own dedicated subsystems (Burch et al., 2016).

To enhance the absolute duty cycle rate for the MMS plasma 3-D data products, the multiple sensor approaches of the ISEE-1 VES (Ogilvie & Scudder, 1979) and the Polar Hydra (Scudder et al., 1995) instruments were generalized in the MMS design to allow DES and DIS duty cycles for 3-D moments to be below the MMS spacecraft 20 s spin period.

The DES and DIS subsystems measure particle fluxes in three dimensions, each with two pairs of electrostatic analyzers, and have *different*, *commensurate*, but *asynchronous*, duty cycles Δt_{DXS} for their respective 3-D moment products. As launched the DIS 3-D moment data product duty cycle is 5 times slower than that of the DES electron data products (Pollock et al., 2016); as flown in its routine *burst mode* the DES had

a duty cycle $\Delta t_{DES} = 30$ ms, while the DIS duty cycle was $\Delta t_{DIS} = 150$ ms. This should be compared with Figure 1b where typical electron skin depth transits have 35 ms durations.

The implications of these hardware choices are illustrated in Figure 2 against the backdrop of a time resolved current density profile expected from skin depth effects; its chosen parameters are typical of the noon magnetopause, reflecting the mode of transit time $\mathbb{TT}$ suggested by Figure 1b. The adopted skin current profile is identical in the two panels of Figure 2; the panels contrast and compare the acquisition times for DXS data products in two different ground processing data formats: *burst* and *qburst*, in Figures 2a and 2b, respectively. At launch (Pollock et al., 2016) and throughout the mission, the default data format for moments is the burst mode. In late 2017, first mention is made of the existence of qburst data products by Torbert et al. (2017) which were subsequently documented by Rager et al. (2018). In late 2020, Project Scientist Giles confirmed that most archived MMS data products were produced in the slower, burst format.

For both panels of Figure 2, contiguous, juxtaposed time intervals have been indicated by rectangles (color coded blue for DIS and red for DES). The widths of each rectangle depict the programed time for DXS to collect fluxes in energy and angle to enable *one* set of 3-D moments to be determined by numerical integration *for that subsystem in that data format*. The time tag for each rectangle is midway along the t axis within each rectangle.

These rectangles in both panels (red [DES] and blue [DIS]) illustrate that there are no holes in *time coverage* of the DXS subsystems. However, these same panels show that the *time resolution* of that complete time coverage is much higher for the DES than the DIS. Regardless of data format, this visualization of data products demonstrates that the DXS data replication rate, or frequency, for the DES is *always* 5 times higher than that for the DIS. In the language of information theory, this fact implies that the Nyquist frequency for DIS data products is *always* 5 times *smaller* than that for the DES. In very practical terms, this ratio of Nyquist frequencies implies that the intrinsic time domain frequency resolution for DIS observations is coarser than that of the DES in the same data format.

Also important is the fact that DES and DIS data acquisition intervals are *commensurate*, so that there is a precise group of five DES data acquisition intervals nested within each *single* DIS acquisition interval. It will soon be important to realize that the periodic absolute time where this 5:1 correspondence starts anew is indicated by the periodic cyan ticks above and below the red and blue rectangles. In general, as here, these tags of commensurability will not occur at the peak of the skin current layer encountered. This implies that getting the appropriate $\mathbb{J}2, \mathbb{J}1$ that are monotonic for the scale length measurements could be as much as Δt_{DIS} away (with lower current densities) from the peak current region, making the current density determination more difficult than if this phasing where assumed locked to the peak skin current traversal.

These *patterns* of the DES and DIS data acquisitions shown in Figure 2 reflect the as built hardware; they are sufficient to prove Theorem II (below) about the minimum data acquisition interval and hence time cadence $\Delta\tau$ for determining current density **J** in a model-independent way.

Since the MMS FPI approach aims to measure **J** via Maxwell's definition by subtracting the electron number flux from that of ions, an important scientific question is the recipe for producing current density **J** data products from the always asynchronous DES and DIS data products illustrated in Figure 2. Neither the experiment description (Pollock et al., 2016) nor subsequent science papers have addressed how the current densities used for published MMS scientific conclusions could be computed from the asynchronously deployed plasma subsystems.

Maxwell defined $\mathbf{J}(t)$ as the simultaneous sum of charged particle fluxes:

$$\mathbf{J}(t) \equiv\mid e \mid \left(\Sigma_k n_k(t) Z_k(t) \mathbf{U}_k(t) + Z_e n_e(t) \mathbf{U}_e(t)\right), \tag{7}$$

where k runs over the indices of all ion species of different charges Z_k, density n_k and 3-D flow velocity $\mathbf{U}_k$. To determine the current density of Maxwell requires values for the 3-D charge number fluxes, $n_q Z_q \mathbf{U}_q$, for *all* species q in the plasma. (In principal, this also requires the need for measurements of densities and flow velocities for *all* ions that have different mass per unit charges! As discussed below these requirements are ignored when reporting $\mathbf{J}_{particle}$.)

Caveat: To examine the critical issue of FPI's asynchronous time tags, this paper focuses on the consequences of the FPI *idealization* that supposes all DIS counts were caused by protons (Pollock et al., 2016) and the DES only measured electrons. (The DIS is an energy per unit charge spectrometer that admits positive ions to be counted provided they have the correct mean values of two polar angles and the tuned kinetic energy per unit charge. Although neither omnipresent alpha particles nor O^+ are excluded from such measurements near the magnetopause, they are not accounted for in the FPI analysis [Pollock et al., 2016].) *All the findings below are predicated on the appropriateness of the above approach to processing the DIS count rates. Fulfilling the necessary conditions outlined in the theorems below may not still give model-independent current density reasons if these assumptions are unwarranted*. The linearity of Equation 7 ensures that if, as with plasma measurements, only time averaged charge moment number fluxes of any species are measurable, then the only measurable current density is the sum of the *corresponding* time averaged quantities, $< >_A$, of the respective terms in Equation 7 yielding:

$$< \mathbf{J} >_A \equiv \mid e \mid \left(\Sigma_j < n_j Z_j \mathbf{U}_j >_A - < n_e \mathbf{U}_e >_A \right). \tag{8}$$

Because averaging involves integration, it is a linear operator, leaving the additive structure of Equation 7 preserved in Equation 8 *when the limits of time averaging (integration) are the same for all quantities averaged*.

Though asynchronous, the DIS and DES sensors on MMS have duty cycles that are rational multiples of one another (cf. Figure 2). The *first* place where the spirit of Maxwell's **J** can be implemented with analog observables is by defining the average operator as the average over the time interval of the slower DIS duty cycle; this would identify the DIS data products as their measured value on the DIS time scale (with aliasing interval Δt_{DIS}). In the same process, DES($t_{e,jk}$) data products must be replaced by their time average of over $k = \{1, 5\}$ electron readings with time tags $t_{e,jk}$, that were recorded during one DIS data product, centered at t_j, viz.

$$\overline{n_{e,j}} \equiv \Sigma_{k=1}^{5} \frac{n_e(t_{e,jk})}{5} \tag{9}$$

$$\frac{\mathbf{J}(t_j)}{\mid e \mid} \equiv \Sigma_\ell Z_\ell n_\ell(t_j) \mathbf{U}_\ell(t_j) - \frac{\Sigma_{k=1}^{5} n_e(t_{e,jk}) \mathbf{U}_e(t_{e,jk})}{5}. \tag{10}$$

This expression assumes that all ion fluxes are known on the DIS measurement duty cycle. They never are (Pollock et al., 2016).

The standard FPI processing for the DIS postulates all flux comes from protons (Pollock et al., 2016) unpacks a phase space density labeled f_p, as if it were the actual proton velocity distribution function, and using Equation 16 for **J** at the DES cadence making, all told, *three additional approximations* to Equation 10:

(i) Assuming the *effective phase space density* for the measured DIS fluxes is

$$f_p(\mathbf{v}_p(i,j,k)) \equiv G(i,j,k) C(i,j,k) \,/\, v(i)_p^4, \tag{11}$$

where the i, j, k indices span the energy per charge steps and two polar angles steps inventoried during the measured DIS flux acquisition, and $v(i)_p$ is the *proton speed* at the energy center of the ith energy per charge channel. $G(i, j, k)$ are the assigned phase space factors measured from preflight calibration, including accumulation time for the step (i, j, k). The approach ignores the energy per unit charge acceptance properties of the DIS subsystem. To our knowledge, the errors of this assumption are nowhere inventoried in the literature.

(ii) It *defines* the center of "ion" flow vector $\mathbf{U}_i$ from DIS as

$$\mathbf{U}_i(t_j) \equiv \frac{\int f_p(t_j) \mathbf{v} d^3 v}{\int f_p(t_j) d^3 v}, \tag{12}$$

and

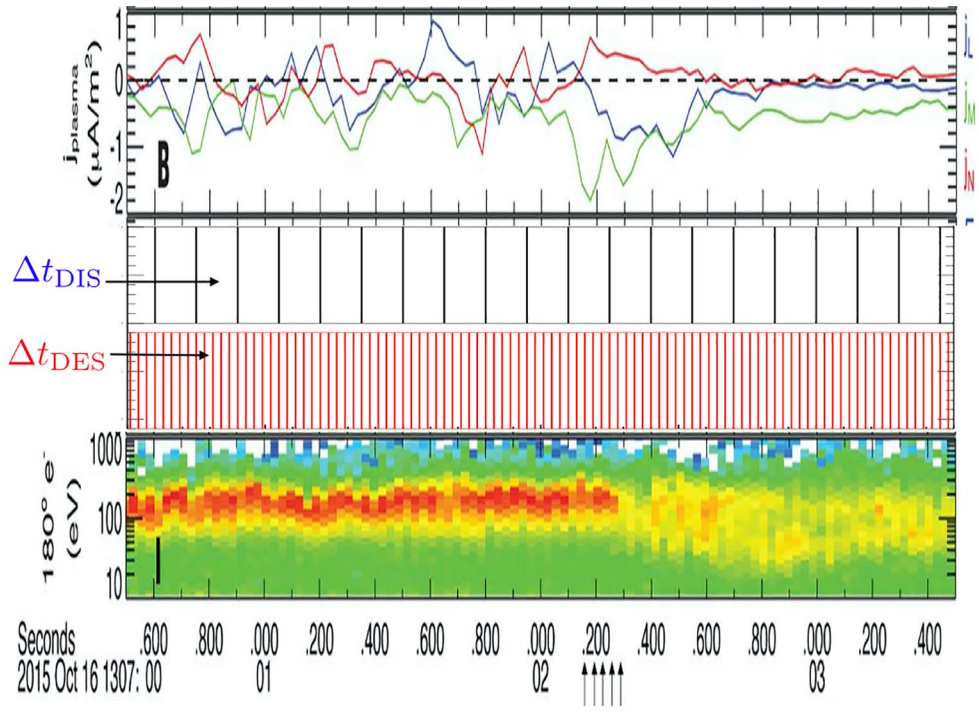

Figure 3. Upper and lower panels are from Figures 4B and 4I of Burch et al. (2016). The middle two rows of rectangular grids have widths to scale of the DIS (black) and DES (red) readings for this burst mode data. Comparing the red rectangle widths with the step like columnar form of the electron spectrogram in the lower panel verifies this association. Disconcertingly, the analyzed signatures of $\mathbf{J}_{plasma}$ clearly possess structure above the highest frequency that the ions have been sampled (centers of black rectangles).

(iii) defines

$$n_i(t_j) = \overline{n_{e,j}} \neq \int f_p(t_j) d^3v, \tag{13}$$

a contradiction of the assumptions implicit in defining f_p. If the f_p construction *were* self-consistent, its phase space density would numerically determine the proton number density n_p, and if it *were* the appropriate DIS approximation it should numerically be the total ion charge density and thus independently correspond to the electron charge density:

$$\int f_p(t_j) d^3v \equiv n_p(t_j) \equiv \overline{n_{e,j}} \tag{14}$$

Figure 3 in Haaland et al. (2020) shows that the required consistency check in Equation 14 is not seen with the routine MMS data processing.

Under the assumptions of FPI data processing (Pollock et al., 2016), Equation 10 might then be approximated as

$$\frac{\mathbf{J}(t_j)}{|e|} \simeq \overline{n_{e,j}} \left(\mathbf{U}_i(t_j) - \frac{\Sigma_{k=1}^{5} n_e(t_{e,jk}) \mathbf{U}_e(t_{e,jk})}{5\overline{n_{e,j}}} \right), \tag{15}$$

where the $t_{e,jk}$ are the five center times (of the red DES rectangles in Figure 2) during the jth DIS reading. Subtracting the average of the DES electron products across the DIS aliasing interval from the ion flow vector reading centered at t_j approximates a current density $\mathbf{J}(t_j)$. The development for Equation 15 proves Theorem II:

Theorem II. "The $\Delta\tau$ of Theorem I for the as flown MMS FPI instrumentation is the minimum time interval necessary to accumulate fluxes (of the data format in use) for one, model-independent 3-D moment determination from the DIS subsystem (assuming its default data processing assumptions; Pollock et al., 2016); this implies $\Delta\tau = \Delta t_{\rm DIS}$ in all data formats." This minimum time could even be as long as the time to include 3-D composition before such determinations were truly model independent. In that circumstance, $\Delta\tau$ would correspond to the first period of recursion of all measurement systems involved. This minimum $\delta\tau$ is thus 150 and 37.5 ms for burst and qburst data format products, respectively. Equation 15 restates the substitutions with FPI data processing that might first approximate the intent of Equation 10 to measure a "model independent" Maxwell current density. Below we show that the MMS data product $\mathbf{J}_{\rm plasma}$ is presented *as measured and model independent* at the much faster DES cadence that are 30 and 7.5 ms in burst and qburst data formats (cf. Burch et al., 2016 and Figure 3).

3.1. An Ad Hoc Expression

$$\mathbf{J}(t_{e,ik}) \simeq |\, e \,|\, n_e(t_{e,ik})\Big(\overline{\mathbb{U}}_i(t_{e,ik}) - \mathbf{U}_e(t_{e,ik})\Big). \tag{16}$$

for $\mathbf{J}$ at the DES cadence can be constructed by making *one further approximation* beyond those in Equations 11, 13 and 12 to Equation 10: proscribe a *recipe* for determining from the slower DIS cadence of $\mathbf{U}_i(t_j)$ the *inferred and unmeasured* vectors, denoted as $\overline{\mathbb{U}}_i(t_{e,jk})$, for the flow velocity of the center of ionic charge at the faster DES cadence time tags $t_{e,ik}$.

Equation 16 is never used in the MMS literature. A less than complete form, Equation 17, is repeatedly used in publications (e.g., Burch et al., 2016; Phan et al., 2016, 2018; Webster et al., 2018):

$$\mathbf{J} \simeq |\, e \,|\, n_e\big(\mathbf{U}_i - \mathbf{U}_e\big). \tag{17}$$

Comparing Equation 17 without explicit declaration of time dependence with Equation 10 where time labels are explicitly declared for the terms presented, results in obscuring that the cited ion $\mathbf{U}_i$ and electron $\mathbf{U}_e$ measurements are only available at *different* times as clearly indicated in Equation 10. By the conventions of typesetting, Equation 17 *implies* that the *functional dependence* of variables on the right-hand side are the same as those on the left, implying that all quantities are known at the same time and location. Using the same variable name $\mathbf{U}_i$ as the reported DIS ion flow moment is at the minimum misleading, but on the other hand is not true if $\mathbf{U}_i$ and $\mathbf{U}_e$ are *measured*, rather than computed values by some undocumented recipe.

MMS science papers routinely cite Equation 17, but plot and discuss $\mathbf{J}(t)$ at the faster DES cadence (e.g., Burch et al., 2016 in Figure 4b; Burch & Phan, 2016 in Figures 5e and 5f; Phan et al., 2016, in Figures 1, 3m, and 4r–4t; Phan et al., 2018 in Figure 3; Torbert et al., 2017 in Figures 3a–3c right column; Webster et al., 2018 in Figure 7).

Top and bottom panels of Figure 3 show figure insets from the MMS Science first results paper separated by rectangular grids of the DES and DIS 3-D data availability.

The upper panel depicts the three components of the published MMS data variable labeled as $\mathbf{J}_{\rm plasma}$; it *puzzlingly* possesses much higher frequency content than the estimates (that occur once per black rectangular grid) of the ion flow velocity *measured* by the DIS. The connect-o-dot plot for $\mathbf{J}_{\rm plasma}$ in the upper panel has corners with a frequency at the availability of DES moment quantities as can be seen with the centers of the red rectangles in this figure. The $\mathbf{J}_{\rm plasma}$ properties shown here at the DES cadence are plotted and interpreted in almost all MMS papers. They and their interpretations are invalid and are shown below to be inconsistent with Nyquist's theorem from information theory.

The first results papers and those shown in Figure 3 demonstrate an unjustified reliance on an algorithm's *synthesis* at the DES cadence of the mean ion flow velocity *vectors*, $\overline{\mathbb{U}}_i(t_{e,jk})$. Hidden in this approach is the assertion that the entropy created by the DIS flux averaging performed by the data collection can be undone by the algorithm used.

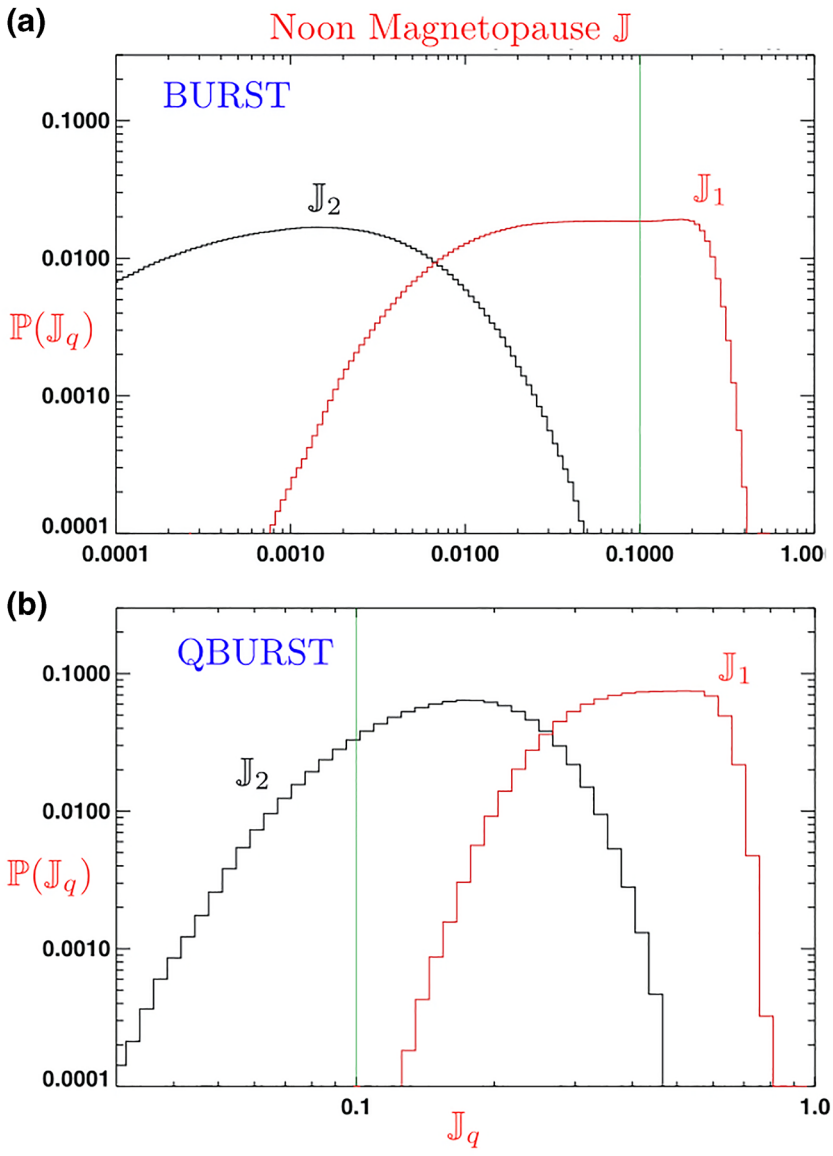

Figure 4. (a) Burst data format and (b) Qburst data format. Green line average current 10% of peak current.

4. Theorem III: J at DES Cadence

In this section, we proceed to demonstrate that the MMS $\mathbf{J}_{\text{plasma}}$ signatures reported and interpreted as measured at the cadence of the DES plasma subsystem of FPI violate the foundations of information theory in the form of Nyquist's theorem.

Assume provisionally that the FPI assumptions (Pollock et al., 2016) allow DIS ground software to produces the time averaged center of ion charge velocity $\mathbf{U}_i(t_j)$. If DES cadence ion flow values, $\overline{\mathbb{U}}_i(t_{e,jk})$, were knowable at the five intermediate DES times ($t_{e,jk}$, $k = \{1, 5\}$), then by quasi-neutrality each of these (proton only) flow vectors would be accompanied by a charge density equal to that $n_e(t_{e,jk})$ as *measured* by the DES at the corresponding time, $t_{e,jk}$:

$$n_i(t_{e,jk}) \equiv n_e(t_{e,jk}). \tag{18}$$

For a given DIS ion measurement, each of its three observed cartesian components ($m = \{x, y, z\}$) for ions, $U_{i,m}(t_j)$ constrain the five hypothesized unknowns, $\mathbb{U}_{i,m}(t_{e,jk}), k = \{1, 5\}$ that are ostensibly the 5, mth components of the ion flow velocity counterparts to $\mathbf{U}_e(t_e, jk)$ at the DES cadence. These hypothesized components must then *separately* satisfy:

$$
\begin{aligned}
U_{i,x}(t_j) &\equiv \frac{\Sigma_k n_e(t_{e,jk})\mathbb{U}_{i,x}(t_{e,jk})}{\Sigma_k n_e(t_{e,jk})} \\
U_{i,y}(t_j) &\equiv \frac{\Sigma_k n_e(t_{e,jk})\mathbb{U}_{i,y}(t_{e,jk})}{\Sigma_k n_e(t_{e,jk})} \\
U_{i,z}(t_j) &\equiv \frac{\Sigma_k n_e(t_{e,jk})\mathbb{U}_{i,z}(t_{e,jk})}{\Sigma_k n_e(t_{e,jk})}.
\end{aligned}
\tag{19}
$$

Each component equation in Equation 19 has *five* unknowns. Since each constraining equation is a many to one linear mapping, algebra implies there are no unique solutions for the hypothesized $\mathbb{U}_{i,m}(t_{e,jk}), k = \{1, 5\}$. This nonuniqueness reflects the loss of information, the entropy in the DIS readings, since they are averages over their total collection time Δt_{DIS} that spans all the separate five electron collections time intervals $t_{e,jk}$ for which values of $\overline{\mathbb{U}}_i(t_{e,jk})$ are desired.

Accordingly, the slower observations of $\mathbf{U}_i(t_j)$ recorded by DIS cannot *uniquely* determine values for $\mathbb{U}_{i,m}(t_{e,jk})$. As a result, there is no unique ion flow inference possible at the DES cadence from FPI plasma measurements for possible use in Equation 16. While there are an infinity of solution 5-tuples to Equation 19 possible, none is unique. Thus, no one of those guessed solutions can be argued to have allowed $\mathbf{J}$ to be measured in a *model-independent* way, using Equation 16 at the DES cadence. This construction concludes the proof of:

Theorem III. "The Maxwell current density $\mathbf{J}$ [Equation 7] cannot be measured in a model-independent way by the Fast Particle Instrument on MMS at the cadence of the electron plasma subsystem DES, even by assuming all ions collected by DIS are protons (Pollock et al., 2016). Thus, reported values for $\mathbf{J}_{\mathrm{plasma}}$ at 30 and 7.5 ms are not model independent using *burst* or *qburst* data products, respectively."

5. Violating Nyquist's Theorem

The cartesian components of Equation 19 involve hypothesized relationships between observables pertaining to times within one DIS data collection duty cycle. From answers given to inquiries at AGU meetings, there are indications that the DES cadence MMS $\mathbf{J}_{\mathrm{plasma}}$ values reported in the refereed literature are the result of interpolations of DIS measured variations of $\mathbf{U}_i(t_j)$ to intermediate times of the DES cadence electron fluxes. Because the MMS recipe for constructing $\mathbf{J}_{\mathrm{plasma}}$ is unknown, its inferred ion flow values may not even be consistent with being one of the nonunique solutions for Equation 19. Whatever the recipe, it may be summarized as a deterministic, but still essentially arbitrary, way to leverage slower DIS cadence measurements to determine *interpolated* higher frequency DES cadence values like $\overline{\mathbb{U}}_i(t_{e,jk})$ needed to use Equation 16. Because such a recipe is for the purpose of increasing the time resolution of $\mathbf{U}_i(t_i)$, they represent attempts to construct the *unmeasured* higher frequency content of the ion flows *beyond those measurements placed in telemetry by the* DIS.

The measured DIS flow observations determined from telemetry are periodic. From information theory, Nyquist's theorem (Haykin & VanVeen, 2003) says it is impossible from periodically sampled data to infer uniquely the higher frequency content of the parent (underlying) continuous function from which the periodic samples were extracted. This theorem, usually proved by Fourier methods, is an impossibility theorem, also relevant for other approaches to possibly infer super Nyquist frequency information, such as interpolation, or finite difference trees, etc. The *unmeasured* values for $\overline{\mathbb{U}}$ that properly correspond to the shorter aliasing interval for the DES reported observations are not uniquely available from slower DIS telemetry; that is the content of the Nyquist theorem.

The critical point is that hardware specifications, not the data variability, set the Nyquist condition for DIS *in all data formats* to be 5 times smaller than that for DES. The Nyquist theorem says it is impossible to infer the true (and thus model independent) high-frequency content of the parent distribution of the ion flows at frequencies above the DIS sampled ion Nyquist frequency. Clearly to reach the frequency domain of DES, one needs to create (since MMS did not measure) the time domain structure in the parent distribution above its (the DIS) Nyquist frequency. The DIS data have an intrinsically lower frequency content; therefore, Taylor series, splines, or other mathematical formulae cannot infer the missing higher frequency content of the underlying parent ion flow distribution.

It should be carefully noticed that whatever approach used by MMS only computes preferred values by the selected method; Nyquist precludes these numbers from being *the* unique measure of the ion flow velocities at the higher DES cadence. Thus, Nyquist's theorem precludes the reliability or uniqueness of interpolation of DIS data to a DES cadence in evidence in the top panel of Figure 3 and the MMS literature; the theorem therefore precludes the physical relevance of such a computation being a unique model-independent measurement of the **J** at the DES cadence as is implied by MMS science publications.

Particularly, troubling about the nonuniqueness of the reported $\mathbf{J}_{\text{plasma}}$ construction is that the precise prejudices of the nonunique promotion of DIS data samples to a DES cadence may easily make different errors on different cartesian components of **J**, causing the inferred current density at the DES cadence to not even be parallel to the true ambient current density. Such approaches can also easily be shown (cf. Appendix A) to cause current densities $\mathbf{J}_{\text{plasma}}$ to be inferred when no physical current densities are present. Unfortunately, such considerations cast shadows over MMS reports and scientific interpretations of geometrical quantities involved in identifying transits of reconnection sites; among these quantities are the size or sign of

$$J_{\|}E_{\|} \quad \text{or} \quad \mathbf{J}\cdot\left(\mathbf{E}+\mathbf{V_e}\times\mathbf{B}/c\right). \tag{20}$$

At present, these reported MMS quantities are not model independent, nor a defensible basis for reports of scientific discovery.

6. To Measure Inertial Scale Length J

Vasyliunas's suggestion was that **J** bounding the EDR should occur *possessing electron inertial scales*. Using the skin depth current profile of Figure 2 for specificity, the time averages performed by the FPI instrumentation (indicated by $< >$) of the current density $| < \mathbf{J}(t_q) > |$ across two adjacent DIS time tags t_1 and t_2 are given by

$$\begin{aligned}\mathbb{J}_1 \equiv \frac{|\langle J_1\rangle|}{|J_o|} = \frac{\mathbb{TT}}{\Delta t_{\text{DIS}}}\exp\left(-\frac{\eta\Delta t_{\text{DIS}}}{\mathbb{TT}}\right)\times \\ \left[1-\exp\left(-\frac{\Delta t_{\text{DIS}}}{\mathbb{TT}}\right)\right] \quad 0\le\eta\le 1\end{aligned} \tag{21}$$

$$\mathbb{J}_2 \equiv \frac{|\langle J_2\rangle|}{|J_o|} = \exp\left(-\frac{\Delta t_{\text{DIS}}}{\mathbb{TT}}\right)\frac{|\langle J_1\rangle|}{|J_o|} \tag{22}$$

where η is the fraction of Δt_{DIS} that the first DIS data collection is delayed commencing after passing the peak of the skin depth current layer shown in Figure 2. The current densities normalized to the peak current density J_o at the beginning of the skin depth layer are given a condensed notation $\mathbb{J}_q$ with a subscript that of the time tag's subscript of the averaged current density.

Determining the spatial scale of $\mathbb{J}$ and noting Theorem II, implies

$$L_{\mathbb{J}} \simeq \left|\frac{V_{MP}\Delta t_{\text{DIS}}}{\ln \mathbb{J}_2/\mathbb{J}_1}\right| = V_{MP}\mathbb{TT} = d_e, \tag{23}$$

showing that the time averages over the skin depth profile involved in the plasma instruments data collection do not deter those data products from retaining the spatial scale information of the unaveraged skin current profile shown in Figure 2.

However, this construction clearly shows that two time adjacent, measurable, and independent current densities must be available to determine a first finite difference measurement of the scale length represented by observations of a current channel. (Note that this circumstance also requires a detectable current density on both steps; otherwise the denominator of Equation 23 is not available for assay.) The above constitutes a constructive proof of an amplified statement of the first theorem:

Theorem IV. "The fastest possible certification of an *inertial scaled* current density using MMS plasma observations is at the cadence of $\Delta\tau = 2\Delta t_{DIS}$, and then only in the approximation that all ions collected by DIS are assumed to be protons. These measurements are potentially available at duty cycles no faster than 300 or 75 ms for burst or qburst formats, based on model independent, monotonic, successive, detections of **J** based on Equation 15." Meaningful determinations depend on the propagation of errors for the determinations of $\mathbb{J}_q$.

7. Which Data Formats Work at Noon MP?

Given the theoretical constraints of the theorems above on model-independent **J** measurements, it is of interest to see what the near noon magnetopause parameters of Figures 1a and 1b imply for detectability first (i) of current density, **J** and second (ii) of *inertial scaled current density* across data formats. It is the second observable that impacts the MMS research area of the EDR of CMR, since it provides the *marker* of the circumstances Vasyliunas envisaged as diagnostic of the EDR environs.

Using Equations 21 and 22 and the parameter probabilities shown in Figures 1 and 4a and 4b show the probability distributions $\mathbb{P}(\mathbb{J}_q)$ for values of $\mathbb{J}_1$ (red) and $\mathbb{J}_2$ (black) for burst (a) and qburst (b) data formats. All other parameter variations included are further manipulated by picking η in Equation 21 as a uniform random variable between 0 and 1 to mock up the sizes of time averaged currents based on the chance phases of initiating a DIS measurement cycle after transiting the current peak.

The presented data are normalized probabilities of occurrence $\mathbb{P}(\mathbb{J}_q)$ given the parameters of Figures 1a and 1b and trials of η for each possible combination of expected observables.

In Figure 4a, for burst mode, the distribution of $\mathbb{J}_1$ is shown to be broad, but generally below 0.3, while still well above all values for the next lower possible observation distribution for $\mathbb{J}_2$ shown in black. This strong reduction reflects the expected time average current reduction caused by the factor $\exp(-\Delta t_{DIS} / \mathbb{TT})$ in Equation 22. In burst format $\Delta t_{DIS} = 150$ ms, while $\mathbb{TT} \simeq 35ms$ this reduction is particularly strong (relative to this effect in qburst format) because of the longer DIS integration times. The green vertical line at 0.1 is used to show with the presented probabilities there is essentially no chance to measure a scale length even for those 27% of encounters where one model-independent measurement of **J** seems possible. Thus, in burst mode, these few observations (27%) of those involved in Figure 1 would all have an vanishingly low chance of being able to measure any scale with such low $\mathbb{J}_2$ mean currents.

By contrast, the qburst format shows nearly 80% of $\mathbb{J}_1$ current channels encountered would allow estimates of scales, provided that the rms variance of the average electron cancellation flux in Equation 22 is smaller than the measured net $\mathbb{J}_2$ current density on the lower step of the decline suggested by Equation 22.

It is worth restating that the Vasyliunas suggestion for markers of the EDR requires a *measurement of scales* and that those scales should compare favorably with the local skin depth computed using the local electron density. Verifying Vasyliunas's picture of the EDR is not possible by measuring a current **J** without showing the measured scale of the current density had an electron inertial length scale.

This overview shows that the best detectability for single current density measurements by percentage of likely opportunities would occur using qburst data format; this format is also most conducive to making a measurement of the scales of the current density.

Unfortunately, qburst data format products are very rare in the MMS data archives and are not used in the first couple years of MMS data analysis. In burst mode, by contrast, virtually none of the conditions appropriate to the noon magnetopause parameters are conducive by this analysis for model-independent meas-

urement of inertial scale length **J** channels. Virtually, all papers published with MMS data since launch, including the initial Science first results and mission success analysis, have been performed with either burst or qburst data, producing $\mathbf{J}_{\text{particle}}$ with an entropy reversing methodology contradicted by Theorem II above and Nyquist's theorem. There is much reanalysis needed to remedy this unfortunate circumstance.

8. Relevance to MMS Data Interpretation

Because a physical quasi-static **J** is always the difference between measured contemporaneous ion and electron charge number fluxes in *all* conditions, the impossibility of measuring **J** at the DES cadence is a reflection of the DIS Nyquist frequency being 5 times smaller than the DES Nyquist frequency for 3-D moments. The relation between these Nyquist frequencies *is fixed by the FPI instrument's hardware and remains so across existing data formats* making this paper's arguments completely independent of the geophysical region where the data were collected. Finally, the time resolution of model-independent **J** measurement is first compatible with Nyquist's theorem and Maxwell's definition of current density when five DES observations that occur during the one contemporaneous DIS observation are averaged *down* to the average cadence of cycles of such DES averages are contemporaneous with the DIS time tag cadence (cf. Equation 15). These conditions directly follow from the specific implementation of the separate DES and DIS subsystem hardware and do not depend on the geophysical regime of the data collection.

The Nyquist condition of a single measurement chain like a magnetometer determines what ambient magnetic field profiles can be recovered from its data time series. In the present paper, the results of the analysis are determined by the effective Nyquist frequency ν_J for the determination of a current density measured according to the Maxwell definition of current density as the difference of two *different* measurement chains [DES, DIS] that each have their own separate Nyquist frequency, ν_{DES} and ν_{DIS}. Figure 2 is a visualization of the disparity of these subsystem-specific Nyquist frequencies. It also implies what the effective ν_J should be for the measurement of current density as the contemporaneous difference of ion and electron number fluxes aliased over the same time interval. Thus, ν_J is synonymous with the Nyquist frequency of the slowest of the subsystems since here they are commensurate at this frequency. Therefore $\nu_J = \nu_{\text{DIS}}$. To measure the spatial scale of **J** requires that the variation of **J** must be measurable at successive opportunities with a time spacing comparable to the expected time transit of the skin depth scale, $\mathbb{TT}$. This implies via Theorem I that $\Delta t_{\text{DIS}} = \mathcal{O}(\mathbb{TT})$. Consulting $\mathbb{P}(\mathbb{TT})$ in Figure 1b for noon magnetopause parameters implies that skin depth currents are not measurable unless

$$\begin{aligned} Burst : 150ms &\simeq \mathcal{O}(35)ms \\ Qburst : 37.5ms &\simeq \mathcal{O}(35)ms, \end{aligned} \tag{24}$$

implying that Nyquist *compatible* model-independent determinations of skin depth scaled current density layers at the noon magnetopause are extremely unfavorable for the common burst mode, but much more likely for qburst mode. Similar conclusions were motivated when discussing Figures 4a and 4b.

Geophysical regimes do influence whether the DIS or DES separately have adequate statistics and thus separately have meaningful measurements; but geophysical regimes do not determine if the electron and ion subsystem measurement *can consistently* cooperate to achieve a measurement product **J** consistent with the measurement entropies of each subsystem. The theorems of this paper have demonstrated that the MMS published quantity $\mathbf{J}_{\text{plasma}}$ at the DES cadence is inconsistent with the measurement entropy of the DIS subsystem. Accordingly, the scientific results derived from such data products have an unknown credibility and most certainly are not model-independent measurements worthy of establishing new physical understanding.

9. Summary

In this paper, eight major points have been established:

(i) The MMS current density $\mathbf{J}_{\text{plasma}}$ at the DES cadence is not model independent.
(ii) The minimum elapsed time for a model-independent measurement of **J** is the duty cycle for the DIS 3-D ion data products.
(iii) The minimal times for **J** are 150 and 37.5 ms in burst and qburst modes, respectively.

(iv) The minimum elapsed time for a model-independent certification for an electron inertial length scaled **J** is twice the duty cycle for DIS 3-D data products.

(v) The minimum cumulative measurement time for determining electron inertial length of **J** layers is 300 and 150 ms in burst and qburst data formats, respectively.

(vi) Model free identifications of electron inertial scale length **J** layers are expected to be very rare in burst data format, but to be accessible approximately 80% of skin depth layer traverses using qburst data format variables.

(vii) Those who wish to use MMS data products for turbulence studies that push the FPI **J** measurements at their highest defensible frequencies and shortest scales should not use the standard MMS $\mathbf{J}_{plasma}$ data products. The true information content in these data is restricted by the Nyquist frequency of the DIS time tags of the data product being used; the desired model-independent value of **J** must be recomputed using Equation 15 to evaluate the highest frequency model-independent current density at 150 or 37.5 ms resolution for burst mode data, or the much rarer qburst mode data products, respectively.

(viii) It is hoped that this paper will encourage a clarification by the MMS principals of in what way $\mathbf{J}_{plasma}$ at the DES time resolution is a model-independent physical ambient current density; the analysis of this paper suggests that this quantity reflects the unstated preferences embedded in the interpolation schemes used to compute it while violating Nyquist's theorem.

Appendix A

As an example of the odd things that can happen when comparing asynchronous measurements, Figure 5 illustrates in inset (a) the collected signal for two detectors that integrate over the *same* input time signal but with different integration times. These two detector are proxies for DIS and DES subsystems on MMS. These outputs are plotted as bar histograms, so that the widths of their integrations are clearly shown by the width of their histogram bar. The blue histogram has the longer integration time that is 5 times longer than that for the red bar. By construction, the area under all red bars within each blue bar equals the area under that blue bar. The total flux perceived in all such red bars is the same as that in the blue bar. If these two measurement systems were measuring electron and ions, respectively, inset (a) would imply there is no net current flow.

The coarse blue histogram in inset (b) replicates the blue histogram of inset (a) with a magnification of the vertical scale. Using piecewise linear interpolation between the centers of each blue bar, a value is assigned to the five red bars within each blue bar. The red histogram reflects this assignment. It would correspond to a recipe that interpolates the blue sensors flux levels at its coarse time tags to become estimates for the blue flows at the red cadence *had they been measured*. This is an example of an algorithm to promote the blue (DIS) sensor's time resolution to that of the red (DES) sensors. Inset (b) also represents an alternate interpolation of coarse blue (DIS) time resolution to that of the red sensor by imagining five equal readings at the red cadence being transferred as an interpolated blue signal at the DES time resolution, but with all interpolated values equal to the height of the blue histogram within its "bar."

Inset C shows three results of subtraction. Two of these subtractions have a time resolution like the red (DES) subsystem of inset (a). The third difference is the cyan colored curve precisely at zero, known at the coarser resolution (indicated by open circles) of the blue (DIS) subsystem in inset (a). This curve has been computed as the difference between the area under the red curve and blue curves in inset(a) determined once per blue bin within inset (a). This corresponds on MMS to averaging the DES measurements *down* to the slower cadence of the DIS to have time commensurate flux readings suitable for unaliased comparison. Note that this difference (in spite of the time averages of the two subsystems) uniformly gets the correct answer for the model problem constructed: 0.

By contrast either of the two attempts to augment the time resolution of the blue sensor of inset(a) when compared with the red histogram of inset (a) generates a spiky difference signal approximating half the mean flow of either sensor as if a relative drift had been detected. The apparent frequency of these pseudo-differences is that of the higher frequency subsystem, because the interpolation to the higher time cadence comes from data that only have lower frequencies. This is an explicit example of trying to circumvent the entropy of the blue signal that integrates longer than the red signal. Nyquist's theorem states that this

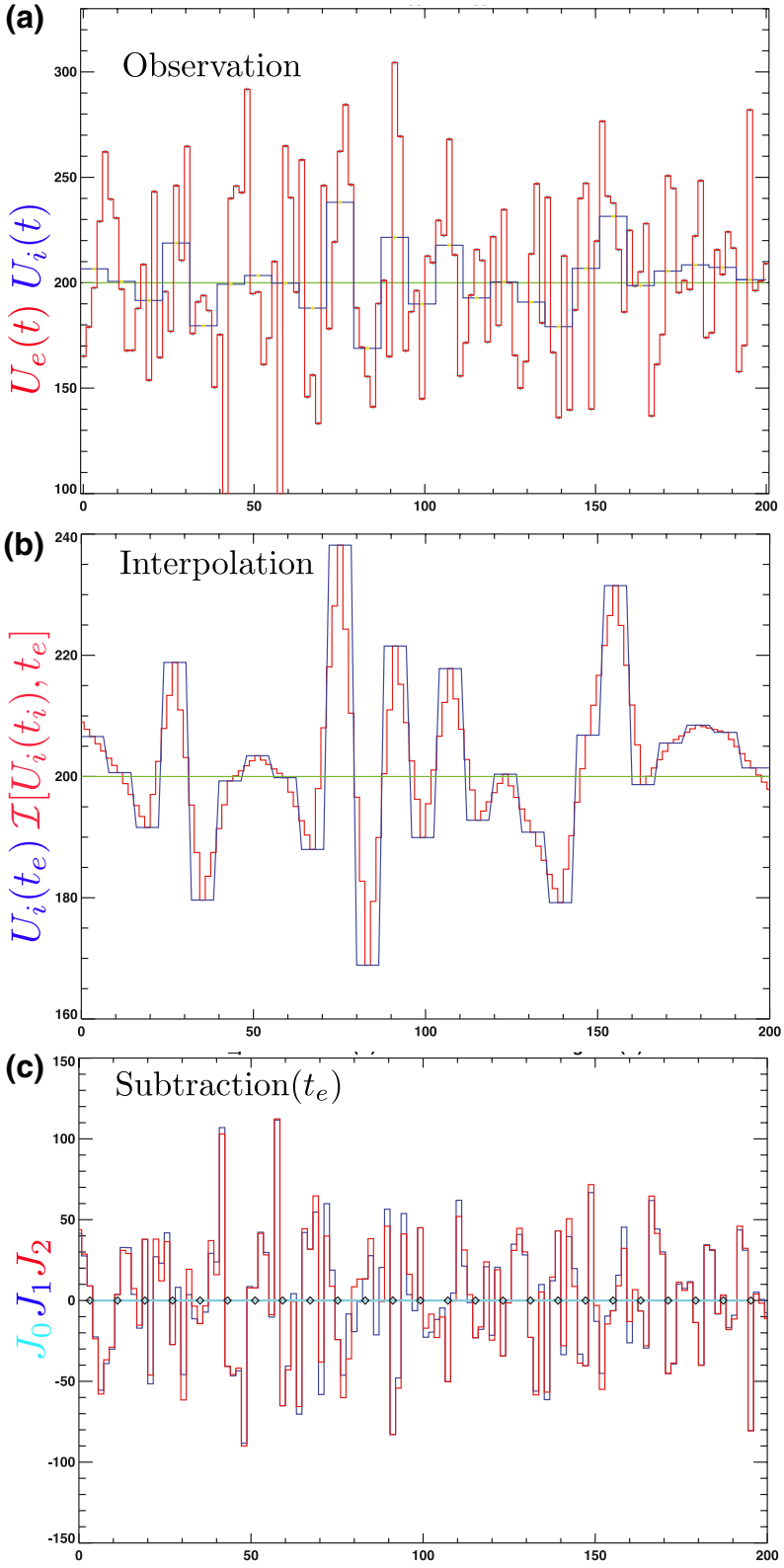

Figure 5. (a) Histogram of one random component of flow seen on DES time scale (red) and the *same* flow component measured during the same time interval on the DIS time scale (blue); (b) interpolations of coarsely time tagged centers of each blue bar of the histogram in (a) to the time resolution of DES; (c) two different estimates of the difference between red (DES) histogram in inset (a) and the interpolated ion flows (blue) in inset (b) and or replicated DIS measurements across the DES cadence.

process cannot be uniquely done. The signature of that lack of uniqueness is that currents are inferred when there are not any present.

In this way, **J** can be inferred when none is present; in other circumstances where a current is present, there is no guarantee that this vector is computed correctly, or necessarily even parallel to the true ambient **J**. If particular components of the current are desired, as in $J_{\|}E_{\|}$, attempts to interpolate to higher frequencies can invent, exaggerate, or even cancel real components of the current along special directions. Accordingly, one time passes through data with such an aliased reconstruction procedure is not conducive to model-independent scientific results.

Data Availability Statement

Data were not used (except quoting or pointing to already published data), nor created for this research. All graphs presented are either original to this paper and derivable from this work or citations of previously published data.

Acknowledgments
The theoretical focus of this paper is understanding the approach adopted to process MMS FPI DES and DIS observations to produce current density at the DES cadence. Lively discussions with MMS principals R. B. Torbert, T. E. Moore, T.-D. Phan, J. C. Dorelli, D. Gershman, and B. Giles are acknowledged. Helpful comments were made by the Editor and the anonymous referees. Funding for this work was partially supplied by NASA grant 80NSSC18K0182.

References

Burch, J. L., & Phan T. D. (2016). Magnetic reconnection at the dayside magnetopause: Advances with MMS. *Geophysical Research Letters*, *43*, 8327–8338. https://doi.org/10.1002/2016GL069787

Burch, J. L., Torbert, R. B., Phan, T.-D., Chen, L.-J., Moore, T. E., Ergun, R. E., et al. (2016). Electron-scale measurements of magnetic reconnection in space. *Science*, *352*, aaf2939. https://doi.org/10.1126/science.aaf2939

Dunlop, M. W., Balough, A., Glassmeier, K.-H., & Robrt, P. (2002). Four-point Cluster application of magnetic field analysis tools: The discontinuity analyzer. *Journal of Geophysical Research*, *107*(A11), 1385. https://doi.org/10.1029/2001JA005089

Haaland, S., Paschmann, G., Oierset, M., Hasegawa, H., Fuselier, S. A., Constantinescu, V., et al. (2020). Characteristics of the flank magnetopause: MMS results. *Journal of Geophysical Research: Space Physics, 125*, e2019JA027623. https://doi.org/10.1029/2019JA027623

Haykin, S., & VanVeen B. (2003). *Signals and systems* (2nd ed.). Hoboken, NJ: John Wiley.

Jackson, J. D. (1975). *Classical electrodynamics* (Vol. 339). New York: John Wiley Interscience.

Khrabrov, A. V., & Sonnerup B. U. Ö. (1998). Orientation and motion of current layers: Minimization of the Faraday residue. *Geophysical Research Letters, 25*, 2373–2376. https://doi.org/10.1029/98GL51784

Ogilvie, K. W., & Scudder, J. D. (1979). First results from the six-axis electron spectrometer on ISEE-1. *Space Science Reviews, 23*, 123–133. https://doi.org/10.1007/BF00174115

Phan, T.-D., Eastwood, J. P., Shay, M. A., Drake, J. F., Sonnerup, B. U. Ö., Fujimoto, M., et al. (2018). Electron magnetic reconnection without ion coupling in Earth's turbulent magnetosheath. *Nature*, *557*, 202–206. https://doi.org/10.1038/s41586-018-0091-5

Phan, T. D., Eastwood, J. P., Cassak, P. A., Øieroset, M., Gosling, J. T., Gershman, D. J., et al. (2016). MMS observations of electron-scale filamentary currents in the reconnection exhaust and near the X line. *Geophysical Research Letters*, *43*(12), 6060–6069. https://doi.org/10.1002/2016GL069212

Pollock, C. J., Moore, T. E., Jacques, A., Burch, J. L., Gliese, U., Saito, Y., et al. (2016). Fast plasma investigation for magnetospheric multiscale. *Space Science Reviews, 199*, 331–406. https://doi.org/10.1007/s11214-016-0245-4

Rager, A. C., Dorelli, J. C., Gershman, D. J., Uritsky, V., Avanaov, L. A., Torbert, R. B., et al. (2018). Electron crescent distributions as a manifestation of diamagnetic drift in an electron-scale current sheet: Magnetospheric multiscale observations using new 7.5 ms fast plasma investigation moments. *Geophysical Research Letters, 45*, 578–584. https://doi.org/10.1002/2017GL076260

Scudder, J. D., & Daughton W. S. (2008). "Illuminating" electron diffusion regions of collisionless magnetic reconnection using electron agyrotropy. *Journal of Geophysical Research*, *113*, A06222. https://doi.org/10.1029/2008JA013035

Scudder, J. D., Holdaway, R. D., Daughton, W. S., Karimabadi, H., Roytershteyn, V., Russell, C. T., & Lopez, J. Y. (2012). First resolved observations of the demagnetized electron-diffusion region of an astrophysical magnetic-reconnection site. *Physical Review Letters, 108*, 225005. https://doi.org/10.1103/PhysRevLett.108.225005

Scudder, J. D., Hunsaker, F., Miller, G., Lobell, J., Zawistowski, T., Ogilvie, K. W., et al. (1995). Hydra—A 3-dimensional electron and ion hot plasma instrument for the POLAR spacecraft of the GGS mission. *Space Science Reviews, 71*, 459–495. https://doi.org/10.1007/BF00751338

Scudder, J. D. (2016). Magnetic reconnection. In W. D. Gonzalez (Ed.), *Astrophysics and Space Science Library 427* (pp. 32–100). Springer. https://doi.org/10.1007/978-3-319-26432-5

Torbert R. B., Burch, J. L., Argall, M. R., Alm, L., Farrugia, C. J., Forbes, T. G., et al. (2017). Structure and dissipation characteristics of an electron diffusion region observed by MMS during a rapid, normal-incidence magnetopause crossing. *Journal of Geophysical Research: Space Physics, 122*, 11901–11916. https://doi.org/10.1002/2017JA024579

Vasyliunas, V. M. (1975). Theoretical models of magnetic field line merging. *Reviews of Geophysics, 13*, 303–336. https://doi.org/10.1029/RG013i001p00303

Wang, C. P., Gkioulidou, M., Lyons, L. R., & Angelopouos, V. (2012). Spatial distributions of the ion to electron temperature ratio in the magnetosheath and plasma sheet. *Journal of Geophysical Research*, *117*, A08215. https://doi.org/10.1029/2012JA017658

Webster, J. M., Burch, J. L., Reiff, P. H., Dou, A. G., Genestreti, K. J., Graham, D. B., et al. (2018). Magnetospheric multiscale dayside reconnection electron diffusion region events. *Journal of Geophysical Research: Space Physics, 123*, 4858–4878. https://doi.org/10.1029/2018JA025245